Received: 4 June 2020 | Revised: 28 November 2020 | Accepted: 1 December 2020

DOI: 10.1002/aic.17166

THERMODYNAMICS AND MOLECULAR-SCALE PHENOMENA

AIChE JOURNAL

Robust and efficient determination of saturation pressure from constant mass expansion data

Mingyuan Wang | Francisco J. Argüelles-Vivas | Ryosuke Okuno

Hildebrand Department of Petroleum and Geosystems Engineering, The University of Texas at Austin, Austin, Texas

Correspondence
Ryosuke Okuno, Hildebrand Department of Petroleum and Geosystems Engineering, The University of Texas at Austin, 200 E. Dean Keeton St., Stop C0300, Austin, TX 78712, USA.
Email: okuno@utexas.edu

Abstract

This article presents an improved method for the determination of saturation pressure from pressure-volume data of constant-mass expansion (CME) for hydrocarbon mixtures. The conventional methods rely on the direct observation of an incipient phase and/or the change in total compressibility of the fluid sample near the saturation pressure in CME; however, they are unreliable for volatile oils, gas condensates, and near-critical fluids. The method developed in this research is to capture the expansion behavior of the overall fluid through the attraction and covolume parameters of the Peng–Robinson equation of state. The reliability of the new method is demonstrated by comparing it with the conventional methods in the case studies using 59 different fluids. It was the only method that could reliably identify saturation pressures for five volatile oils, 11 gas condensates, and one near-critical fluid among the datasets tested.

KEYWORDS
compressibility, constant-mass expansion, hydrocarbon mixtures, perturbation from n-alkane, saturation pressure

1 | INTRODUCTION

Phase behavior of hydrocarbon mixtures plays an important role in petroleum recovery processes. For example, phase separation of oil into the vapor and liquid phases with decreasing reservoir pressure affects the depletion strategy for an undersaturated oil reservoir.[1] In a gas condensate reservoir, the accumulation of liquified condensate near the production wells tends to reduce the gas productivity.[2] Furthermore, the effect of fluid composition on phase behavior is the key mechanism in many enhanced oil recovery (EOR) processes.

Phase behavior of hydrocarbon mixtures is commonly modeled by using a cubic equation of state (EOS).[3] The most commonly used EOSs include the Peng–Robinson and the Soave–Redlich–Kwong equations[4-6] because they are computationally efficient and reasonably accurate for representing hydrocarbon mixtures.[7-9] The attraction and covolume parameters are the inherent parameters in a cubic EOS, and they are usually calculated by using vapor pressure information, such as critical temperature (Tc), critical pressure (Pc), and acentric factor (ω), for each component.[10] Then, the attraction and covolume parameters for a mixture are calculated by the van der Waals mixing rules. Binary interaction parameters (BIPs) can be calculated by correlations or by group-contribution methods.[9,11]

Calculation of the attraction and covolume parameters for well-defined components (e.g., methane, ethane, propane, and carbon dioxide) is straightforward because their vapor pressure curves are known. However, the heavy fractions (e.g., heptane and heavier) in crude oil sample contain a wide variety of compounds. Even for a given carbon number fraction, the paraffin-naphthenes-aromatics (PNA) distribution within the carbon number is highly uncertain.[12] Therefore, such heavy fractions are characterized by using a few "pseudo-components." The attraction and covolume parameters of pseudo-components are adjusted through their Tc, Pc, and ω to match the available experimental data in reservoir fluid characterization.

Different types of experimental data are required in reservoir fluid characterization using an EOS, and the data quality can substantially affect the reliability of the resulting fluid model.[13] Densities and

saturation pressures are important for modeling the volumetric and compositional phase behavior, respectively. One type of saturation pressure is bubble point, which is the pressure at which a vapor phase starts to emerge from the existing liquid phase during isothermal expansion.[14] The other type of saturation pressure is dew point, which is the pressure at which a liquid phase starts to emerge from the existing vapor phase during isothermal expansion.[14] This article is concerned with the reliable determination of saturation pressure from the experimental data obtained by constant-mass expansion (CME).

CME by using a pressure-volume-temperature (PVT) cell is the traditional method of measuring a saturation pressure at a given fluid composition and temperature. A PVT cell is a pressure vessel that is equipped with a piston, a mixer, and a visual window and typically placed in an oven. In CME, a single-phase fluid is injected into a PVT cell at an elevated pressure at the temperature of interest. The initial pressure and volume of the PVT cell are recorded once the fluid sample reaches equilibrium. Then, the pressure in the PVT cell is reduced by expanding the sample volume in a stepwise manner. At each pressure step, the pressure and volume of the fluid sample in the PVT cell are recorded after the sample is mixed and equilibrated.[8]

CME is also used to study the interaction of crude oil and injection gas for gas injection processes for EOR.[7] A series of CME tests for different mixtures of oil and injection gas is called the swelling test.[7,13] The swelling test determines the solubilities of injection gas in reservoir oil at different pressures and the volumetric behavior of the mixtures.[8,13] In a typical swelling test, the fluid in the PVT cell changes from oil to gas condensate with increasing amount of injection gas being injected into PVT cell.[15] Thus, the type of saturation pressure changes from bubble- to dew point with increasing concentration of injection gas. Such swelling test data can contain phase behavior data in a near-critical region, which are important for modeling miscible conditions between the injection gas and the original reservoir oil for gas EOR.[13]

If the PVT cell is equipped with a visual window, an incipient phase can be visually observed in CME. However, this direct observation is often unreliable because it tends to underestimate the true saturation pressure. This issue is particularly common with gas condensate samples because the incipient liquid phase tends to wet the interior of the PVT cell before forming a visible liquid phase.[13,16] Also, visual determination of an incipient phase may be even impossible when the visual window is covered by asphaltene precipitation[13] and when the pressure–temperature conditions for CME make it impossible to use a conventional PVT cell with a visual glass window.

Various methods have been proposed to determine saturation pressure from CME data in the literature.[1,2,17,18] As will be shown in this article; however, the existing methods are often unreliable. The main objectives of this research are to clarify the shortcomings of the previous methods and to develop an efficient and robust method for determining saturation pressure from CME data for a wide range of reservoir fluids. The 59 CME datasets used for this research consist of 15 black oils, 24 volatile oils, and 20 gas condensates as summarized in Tables 1–3. As part of the initial stage of the research, the data quality was confirmed for the 59 datasets as explained in Appendix A.

In the next sections, a discussion of previous methods is followed by the theory and algorithm of the new method for reliable determination of saturation pressure. Then, the case studies present the application of the new method to 59 CME datasets. Finally, the main conclusions of this research are presented.

2 | REVIEW OF PREVIOUS METHODS

Various methods have been developed in the literature for determining a saturation pressure from CME data, such as PV isotherm, extended Y-function, and total compressibility.[1,2] This section reviews these methods and clarifies their common limitation.

The use of experimental PV isotherm is the most conventional method, in which the saturation pressure is given by the breakpoint between the single-phase and the two-phase regions in the PV isotherm data from CME. The slope of the PV data changes depending on the change in total compressibility at the saturation pressure, as shown in the following equation:

$$\frac{\partial V}{\partial P} = -V\left(-\frac{1}{V}\frac{\partial V}{\partial P}\right) = -VC_t, \tag{1}$$

where P, V, and C_t are pressure, total volume, and total compressibility of the fluid, respectively.

The extended Y-function, Y_{EXT}, is defined as

$$Y_{EXT} = \frac{P_i - P}{P_i\left(\frac{V}{V_i} - 1\right)}, \tag{2}$$

where P_i and V_i are respectively the initial pressure and volume for CME.[1] In this method, the logarithm of Y_{EXT} is plotted against pressure, and the breakpoint of the plot is the saturation pressure.[1] This method depends also on the total compressibility as follows:

$$\frac{\partial(\log Y_{EXT})}{\partial P} = \frac{-1}{(P_i - P)\ln 10} + \frac{-\frac{1}{V}\frac{\partial V}{\partial P}}{\frac{(V - V_i)}{V}\ln 10} = \frac{-1}{(P_i - P)\ln 10} + \frac{C_t}{\frac{(V - V_i)}{V}\ln 10}. \tag{3}$$

Total compressibility by itself was used to determine a dew point by plotting it against pressure in the literature.[2] This method relies on the premise that the total compressibility increases at the dew point.[2]

However, these compressibility-based methods have a common limitation as described below. Total compressibility can be expressed by the following equation[2]:

$$C_t = S_E(C_E - C_A) + C_A + \frac{1}{V}\left(\frac{1}{\rho_E} - \frac{1}{\rho_A}\right)\frac{\partial m_A}{\partial P}, \tag{4}$$

where C_E is the compressibility of the exiting phase, C_A is the compressibility of the appearing phase, S_E is the saturation of the existing phase, ρ_E is the density of the existing phase, ρ_A is the density of the appearing phase, and m_A is the mass of the appearing phase. When the existing and appearing phases have a similar compressibility and

TABLE 1 Information of the black oils studied in this research. The slope-ratio values with three different methods are listed, and none of them are between 0 and 2; that is, these black oils are not difficult datasets for the three methods. Slope ratio is defined in the "Review of Previous Methods" section

					Slope ratio		
Fluid No.	Source	Mw, Kg/kmol	Temperature, K	C_{7+} Molar fraction	P-V	$logY_{EXT}$	New method
1	Coats and Smart,[23] oil #6	83.31	385.37	0.3043	5.86	13.17	−15.78
2	Coats and Smart,[23] oil #7	113.60	328.15	0.3597	14.49	50.72	−93.65
3	Danesh[24]	93.75	377.59	0.3329	8.53	22.21	−30.05
4	Jaubert et al.,[25] fluid #1	135.25	374.85	0.4400	24.89	38.84	1,120.85
5	Jaubert et al.,[25] fluid #2	136.25	372.05	0.4580	20.89	32.77	−71.93
6	Jaubert et al.,[25] fluid #3, swelling stage 1	82.42	387.35	0.2902	5.34	9.38	−17.23
7	Jaubert et al.,[25] fluid #3, swelling stage 2	75.48	387.35	0.2579	3.31	7.79	−11.14
8	Jaubert et al.,[25] fluid #3, swelling stage 3	68.65	387.35	0.2262	2.40	7.09	−6.10
9	Jaubert et al.,[25] fluid #4, swelling stage 1	63.17	388.15	0.2127	2.57	4.63	−4.42
10	Jaubert et al.,[25] fluid #11	88.20	373.75	0.2894	3.58	48.81	−38.41
11	Eilert and Smith,[26] separator gas 0 mass%	89.04	382.04	0.4214	29.47	76.20	−107.28
12	Eilert and Smith,[26] separator gas 15.25 mass%	56.59	327.59	0.2277	6.44	9.79	−20.79
13	Eilert and Smith,[26] separator gas 15.25 mass%	56.59	382.04	0.2277	3.45	8.30	−12.20
14	Eilert and Smith,[26] separator gas 15.25 mass%	56.59	410.93	0.2277	3.88	5.33	−10.49
15	Negahban et al.[27]	101.90	394.00	0.3852	11.18	48.16	−31.76

density, the change in total compressibility is small at the saturation pressure. As will be shown later, this is often the case with near-critical fluids and gas condensates. Consequently, the compressibility-based methods are unreliable in determination of saturation pressure for these fluid types and many swelling tests.

The difficulty of compressibility-based methods is demonstrated by the slope change near the saturation pressure as described here. Curve fitting is first performed for the data above saturation pressure ($f_+(P)$) and below saturation pressure ($f_-(P)$). Then, the first-order derivative at the saturation pressure is calculated for both $f_+(P)$ and $f_-(P)$. The slope ratio is defined as $f'_-(P_{sat})/f'_+(P_{sat})$. As the slope ratio becomes smaller, it becomes more difficult to determine saturation pressure. Analysis of the datasets in this research indicated that difficult cases with the PV data and extended Y-function had the slope-ratio values between 0 and 2.

Tables 1–3 present the slope ratios at saturation pressure with PV isotherm and extended Y-function for black oils, volatile oils, and gas condensates, respectively. For PV isotherm, Figures 1–4 show the PV isotherm data of four selected fluids: Fluid #9 in Table 1 (black oil), Fluid #11 in Table 2 (volatile oil), Fluid #18 in Table 3 (gas condensate), and Fluid #8 in Table 3 (near-critical fluid). The volume data were reported as relative volume or specific volume in the literature. For comparison, however, they have been converted to actual volume. The slope change is obvious in Figure 1 with the slope ratio of 2.57, but it is difficult to identify in Figures 2, 3, and 4 with their slope ratios between 0 and 2. The slope ratios indicate that the PV-isotherm method is reliable for determination of saturation pressure for all black oils (Table 1), 13 out of 24 volatile oils (Table 2), and 3 out of 20 gas condensates (Table 3).

Figures 5–8 present $logY_{EXT}$ for the fluids selected previously for Figures 1–4. A clear change in slope is observed in Figure 5, but it is difficult to identify in Figures 6–8. Results indicate that the Y_{EXT} method is more reliable than the PV isotherm method for determination of saturation pressure; that is, it was successful for all black oils (Table 1), 19 out of 24 volatile oils (Table 2), and 8 out of 20 gas condensates (Table 3)

As mentioned previously, use of the total compressibility by itself was proposed for determining a dew point in the literature.[2] Figures 9 and 10 present the total compressibility for Fluid #18 (gas condensate) and Fluid #8 (near-critical fluid) in Table 3. They correspond to fluids in Figures 3 and 4 for the PV isotherm method and Figures 7 and 8 for the Y_{EXT} method. Results show that total compressibility does not show a clear change in slope at the dew point in both figures, concluding that the total compressibility method can be unreliable.

3 | NEW METHOD OF DETERMINING SATURATION PRESSURE

The previous section presented that the prior methods are not generally reliable, especially when the existing and appearing phases have similar volumetric behavior; that is, density and compressibility. This is an inherent problem with near-critical fluids that should be improved by a nontraditional method. The key point of consideration for the new method developed in this research is that the expansion of the overall fluid below the saturation point depends more on the more compressible phase than the other phase; therefore, the expansion

TABLE 2 Information of the volatile oils studied in this research, and the slope-ratio values calculated by three different methods. It is difficult to determine a saturation pressure when the slope-ratio value is between 0 and 2. The difficult datasets are shaded in the table. Out of 24 cases, 11 datasets are difficult with the PV-isotherm method, and five cases with the Y_{EXT} method. None of them is difficult with the new method

					Slope ratio		
Fluid No.	Source	Mw, Kg/kmol	Temperature, K	C_{7+} Molar fraction	P-V	logY_{EXT}	New method
1	Al-Meshari,[28] fluid #16	59.63	425.93	0.1720	1.90	2.18	−6.41
2	Al-Meshari,[28] fluid #17	67.32	414.82	0.1900	1.69	0.53	−3.34
3	Coats and Smart,[23] oil #2	51.11	353.15	0.1692	1.11	3.86	−4.19
4	Coats and Smart,[23] oil #3	70.33	333.15	0.1851	6.86	21.47	−37.59
5	Coats and Smart,[23] oil #3	70.33	344.26	0.1851	5.24	15.66	−33.62
6	Coats and Smart,[23] oil #3	70.33	355.37	0.1851	5.42	11.91	−27.99
7	Coats and Smart,[23] oil #3	70.33	366.48	0.1851	4.60	9.72	−24.29
8	Jaubert et al.,[25] fluid #3, swelling stage 4	62.45	387.35	0.1974	2.11	6.03	−5.05
9	Jaubert et al.,[25] fluid #3, swelling stage 5	56.75	387.35	0.1708	1.75	3.00	−5.12
10	Jaubert et al.,[25] fluid #4, swelling stage 4	48.99	388.15	0.1430	1.60	1.89	−3.87
11	Jaubert et al.,[25] fluid #4, swelling stage 5	45.65	388.15	0.1266	1.37	1.77	−1.94
12	Eilert and Smith,[26] separator gas 29.16 mass%	42.51	382.04	0.1437	1.96	3.23	−11.18
13	Eilert and Smith,[26] separator gas 28.88 mass%	42.72	294.26	0.1449	5.04	13.41	−11.29
14	Eilert and Smith,[26] separator gas 28.88 mass%	42.72	310.93	0.1449	2.35	6.97	−9.98
15	Eilert and Smith,[26] separator gas 28.88 mass%	42.72	327.59	0.1449	3.51	8.06	−8.39
16	Eilert and Smith,[26] separator gas 28.88 mass%	42.72	360.93	0.1449	2.58	3.68	−8.33
17	Eilert and Smith,[26] separator gas 28.88 mass%	42.72	382.04	0.1449	2.33	2.72	−7.51
18	Eilert and Smith,[26] separator gas 28.88 mass%	42.72	410.93	0.1449	2.47	2.48	−8.03
19	Eilert and Smith,[26] separator gas 50.01 mass%	30.99	294.26	0.0749	1.30	4.68	−6.07
20	In-house ethane swelling test stage 1	56.58	347.04	0.1852	1.96	−1.30	9.44
21	In-house ethane swelling test stage 2	54.08	347.04	0.1677	2.29	2.90	−6.97
22	In-house ethane swelling test stage 3	51.55	347.04	0.1500	2.31	5.57	−8.02
23	In-house CME for a mixture of solution gas and live oil	54.91	349.82	0.1217	1.32	0.80	−0.91
24	CME for a mixture of CO_2 and live oil	47.98	349.82	0.1152	1.30	1.77	2.54

for the overall fluid below the saturation point is more representative of the composition of the more compressible, volatile phase. After an exploratory study of various possibilities, a practical method was found that transforms the expansion behavior of the overall fluid (i.e., total compressibility) to compositional behavior information through the attraction and covolume parameters of the Peng–Robinson EOS.

Figure 11 presents an example from an in-house CME experiment for a mixture of 9.5 mol% CO_2 and 90.5 mol% live oil from a shale play in Texas. The expansion of the overall fluid comes mainly from the vapor phase; hence, the volumetric behavior of the overall fluid should require the EOS parameters to represent more volatile fluid as pressure decreases below the bubble point.

Then, the hypothesis tested was that when the volume of the overall fluid is represented by the Peng–Robinson EOS as a single-phase mixture (even below the saturation point), the attraction and covolume parameters should change to represent a more volatile fluid. They are expected to capture the contribution of the more volatile phase to the fluid expansion, which becomes progressively dominant with decreasing pressure. The resulting values of the attraction (a) and covolume (b) parameters are then grouped into a/b^2 to be plotted with respect to pressure. The parameter group, a/b^2, was called the aromaticity parameter by Kumar and Okuno[19] for their fluid characterization method, perturbation from n-alkane (PnA). In this research, plotting the aromaticity parameter with respect to pressure was found to be a convenient method for capturing the compositional effect responsible for the expansion behavior below the saturation point in CME data.

In the new method, the C_{7+} fractions of the hydrocarbon mixture of interest is characterized by the PnA method[9] to match the compressibility factor at each pressure step of CME, using the overall composition (i.e., keeping a hypothetically single-phase below the saturation pressure). Then, the aromaticity parameter, a/b^2, is calculated for each pressure using the attraction (a) and covolume parameters (b) of the Peng–Robinson EOS for the mixture, and it is plotted with respect to pressure. The overall fluid as a single-phase fluid behaves like a less aromatic fluid when the more compressible phase dominates the expansion behavior below the saturation pressure in CME;

TABLE 3 Information of the gas condensates studied in this research. The slope-ratio values calculated by three different methods are listed. The shaded boxes indicate the datasets that are difficult for determining the saturation pressure because the slope-ratio value is between 0 and 2. Out of 20 cases, 17 cases are difficult with the PV-isotherm method, 12 cases with the Y_{EXT} method, and none with the new method

					Slope ratio		
Fluid No.	Source	Mw, Kg/kmol	Temperature, K	C_{7+} Molar fraction	P-V	$logY_{EXT}$	New method
1	Akpabio et al.[29]	27.07	377.04	0.0464	1.16	1.16	−0.34
2	Al-Meshari,[28] fluid #7	36.62	397.59	0.0999	1.13	1.28	−0.54
3	Al-Meshari,[28] fluid #8	40.77	424.72	0.1087	1.43	1.73	−5.14
4[a]	Coats,[30] bottomhole	44.41	435.93	0.1066	2.49	4.20	−5.10
5[a]	Coats,[30] recombined	45.05	435.93	0.1232	5.99	4.14	−8.47
6	Coats and Smart,[23] gas #2 sample #1	44.91	360.93	0.1145	1.27	2.29	−3.41
7	Coats and Smart,[23] gas #2 sample #2	46.15	360.93	0.1220	1.77	3.64	−3.28
8[a]	Coats and Smart,[23] gas #5	30.30	403.71	0.0588	1.08	1.83	−0.85
9	Eilert and Smith,[26] separator gas 50.01 mass%	30.99	327.59	0.0749	1.64	3.32	−3.82
10	Eilert and Smith,[26] separator gas 50.01 mass%	30.99	382.04	0.0749	1.35	1.91	−4.17
11	Eilert and Smith,[26] separator gas 50.01 mass%	30.99	410.93	0.0749	1.54	1.87	−3.66
12	Eilert and Smith,[26] separator gas 73.59 mass%	23.74	294.26	0.0317	1.10	1.90	−0.96
13	Eilert and Smith,[26] separator gas 73.59 mass%	23.74	310.93	0.0317	1.22	1.89	−0.94
14	Eilert and Smith,[26] separator gas 73.59 mass%	23.74	327.59	0.0317	1.12	1.67	−1.11
15	Eilert and Smith,[26] separator gas 73.59 mass%	23.74	344.26	0.0317	1.17	1.51	−0.87
16	Kenyon and Behie[31]	32.61	366.48	0.0659	2.05	2.73	−2.86
17	Sage and Olds[32]	29.35	310.93	0.0576	1.06	2.16	−1.22
18	Sage and Olds[32]	29.35	360.93	0.0576	1.02	1.47	−0.69
19	In-house ethane swelling test stage 4	46.39	347.04	0.1140	1.13	2.08	−60.90
20	In-house ethane swelling test stage 5	41.09	347.04	0.0770	1.28	1.53	−1.79

[a]Near-critical gas condensate.

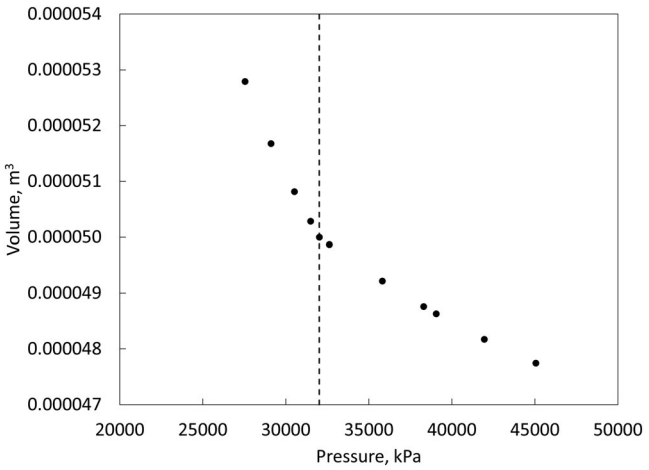

FIGURE 1 Pressure-volume data of fluid #9 in Table 1 (black oil) at 388.15 K[25]. The saturation pressure, which is indicated by the vertical dashed line, is easy to identify with the slope ratio of 2.57

therefore, the aromaticity parameter tends to decrease below the saturation pressure.

The data required for the new method includes the overall composition, the molecular weight of C_{7+}, reservoir temperature, fluid density at a certain pressure in the single-phase region, and pressure-volume data from CME (at least five pressure points as will be discussed later). A stepwise description of the algorithm is presented below.

Step 1: Compositional Characterization. The C_{7+} fraction for the fluid is split into a specified number of pseudo-components by using a chi-squared distribution.[9,20] Four pseudo-components are used in this research.

Step 2: Initial T_C, P_C, and ω for Pseudo-Components. Initial T_C, P_C, and ω values are assigned to the pseudo-components by assuming n-alkanes (or paraffins) by using the following correlations[9]:

$$T_{CP} = \left\{6573.87 - 4680.77\exp\left[-0.1831\left(CN^{0.6667} - 2.08\right)\right]\right\}^{\frac{1}{1.276}}, \quad (5)$$

$$P_{CP} = 4244\exp\left[-0.3757\left(CN^{0.5684} - 1.8672\right)\right], \quad (6)$$

$$\omega_P = 0.217066 + 5.27405CN^{-\left(\frac{14.8147}{CN}\right)}, \quad (7)$$

where CN is carbon number. The subscript "P" stands for paraffins.

Step 3: Incremental Values for T_C, P_C, and ω. The following equations are used to calculate incremental values for T_C, P_C, and ω during the regression[9]:

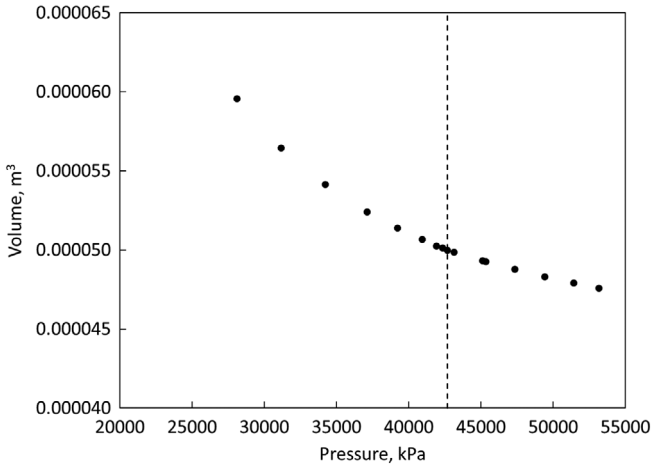

FIGURE 2 Pressure-volume data of fluid #11 in Table 2 (volatile oil) at 388.15 K[25]. The saturation pressure, which is indicated by the vertical dashed line, is difficult to identify with the slope ratio of 1.37

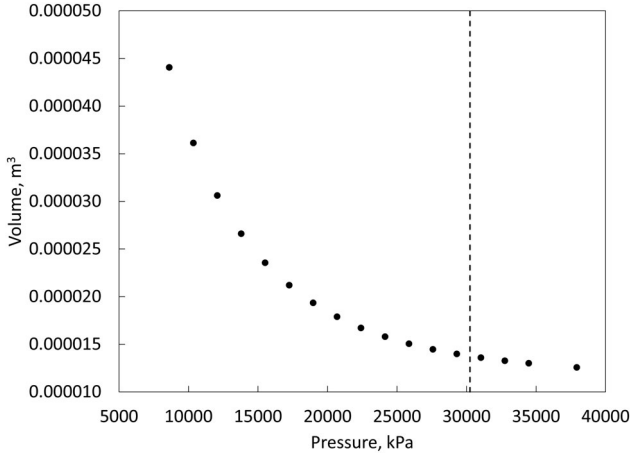

FIGURE 3 Pressure-volume data of fluid #18 in Table 3 (gas condensate) at 360.93 K[32]. The saturation pressure, which is indicated by the vertical dashed line, is difficult to identify with the slope ratio of 1.02

$$\Delta T_{C,i} = (T_{CH,i} - T_{CP,i})/N, \tag{8}$$

$$\Delta P_{C,i} = (P_{CH,i} - P_{CP,i})/N, \tag{9}$$

$$\Delta\omega = \omega_{H,i}/N, \tag{10}$$

for i = 1, 2, ..., n, where N is 10^4 in this research. T_{CH}, P_{CH}, and ω_H are calculated as

$$T_{CH} = 5339.14 - 4850.41\exp\left(-0.001650727669CN^{1.4223}\right). \tag{11}$$

$$P_{CH} = 100\left(48.0823 - 21.7852\exp\left(-11.372937CN^{-1.326532}\right)\right). \tag{12}$$

$$\omega_H = 0.026547\left(0.985567^{CN}\right)\left(CN^{1.295419}\right). \tag{13}$$

Set an iteration-step index k to unity.

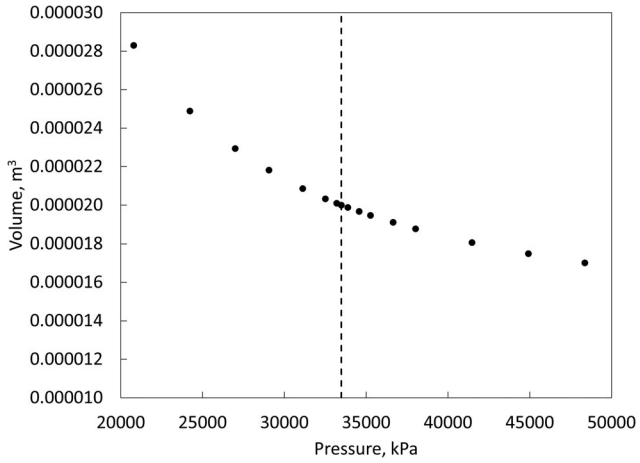

FIGURE 4 Pressure-volume data of fluid #8 in Table 3 (near-critical fluid) at 403.71 K[23]. The saturation pressure, which is indicated by the vertical dashed line, is difficult to identify with the slope ratio of 1.08

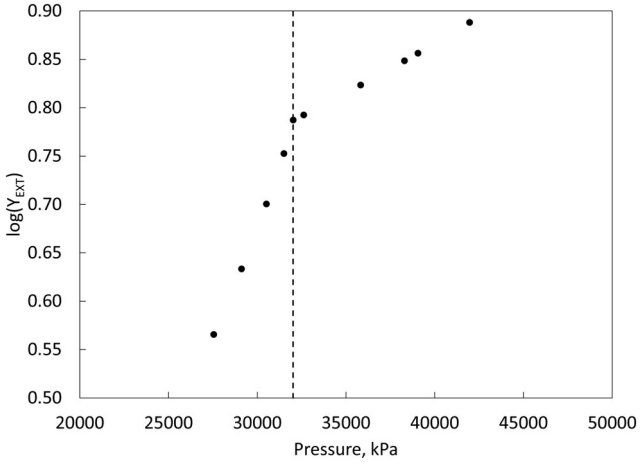

FIGURE 5 $\log(Y_{EXT})$ of fluid #9 in Table 1 (black oil) at 388.15 K[25]. The saturation pressure, which is indicated by the dashed line, is obvious with the slope ratio of 4.63

Step 4: Update of T_C, P_C, and ω. The following equations from Kumar and Okuno[9] are used to update T_C, P_C, and ω:

$$T_{C,i} = T_{CP,i} + k\Delta T_{C,i}, \tag{14}$$

$$P_{C,i} = P_{CP,i} + k\Delta P_{C,i}, \tag{15}$$

$$\omega_i = k\Delta\omega_i, \tag{16}$$

where k is the iteration index.

Step 5: Calculation of Z. The compressibility factor is calculated by solving the Peng–Robinson EOS. The result is denoted as Z_{EOS}.

Step 6: Convergence Test. Calculate $\delta = (Z_{EOS} - Z_{lab})/Z_{lab}$. Z_{lab} is the compressibility factor calculated from CME data.

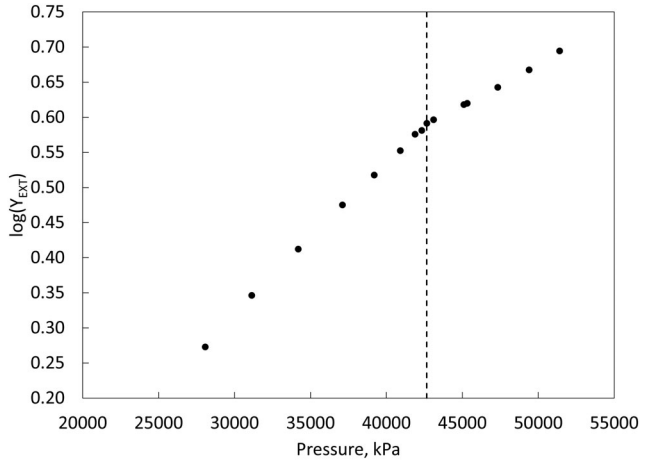

FIGURE 6 $\log(Y_{EXT})$ of fluid #11 in Table 2 (volatile oil) at 388.15 K[25]. The saturation pressure, which is indicated by the dashed line, is difficult to identify with the slope ratio of 1.77

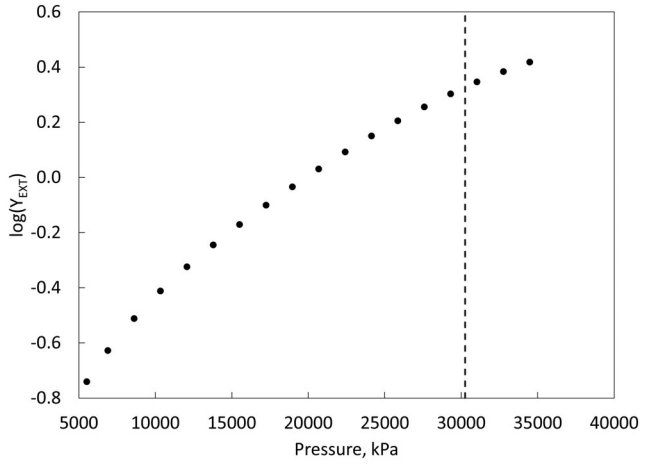

FIGURE 7 $\log(Y_{EXT})$ of fluid #18 in Table 3 (gas condensate) at 360.93 K[32]. The saturation pressure, which is indicated by the dashed line, is difficult to identify with the slope ratio of 1.47

$$Z_{lab} = \frac{PV}{nRT} = \frac{PVMW}{\rho V' RT}, \tag{17}$$

where n is the number of moles, R is the gas constant, T is temperature, MW is the molecular weight of the fluid, ρ is the fluid density at a certain pressure in the single-phase region, and V′ is the volume of the fluid at the same pressure. If $|\delta| < \delta_{TOL}$ (e.g., $\delta_{TOL} = 10^{-4}$), go to step 7. Otherwise, go back to step 4 after increasing k by one.

Step 7: Calculation of Aromaticity Parameter. The aromaticity parameter, a/b^2, is calculated for the mixture.

The fluid characterization as a single-phase fluid, Steps 2–7, are performed for each pressure step of CME. BIPs are calculated by the correlation given by Kumar and Okuno,[9] and not adjusted during the iteration. No volume shift is used because the algorithm is to capture the volumetric behavior through pseudo-components' vapor pressure curves (T_C, P_C, and ω).[21]

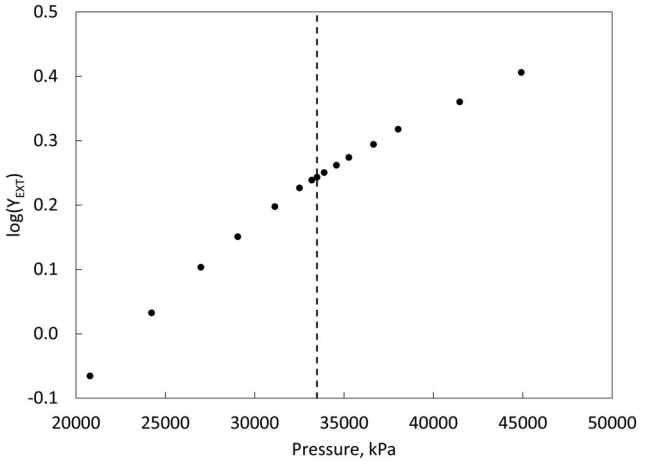

FIGURE 8 $\log(Y_{EXT})$ of fluid #8 in Table 3 (near-critical fluid) at 403.71 K[23]. The saturation pressure, which is indicated by the dashed line, is difficult to identify with the slope ratio of 1.83

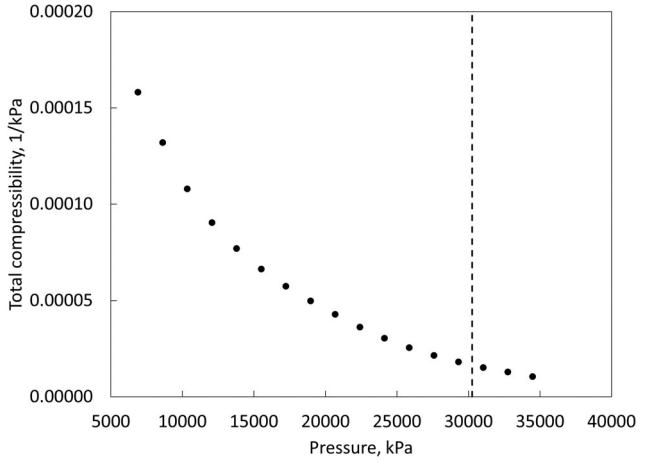

FIGURE 9 Total compressibility of fluid #18 in Table 3 (gas condensate) at 360.93 K[32]. The saturation pressure is indicated by the dashed line. Total compressibility does not show a clear change in slope at the dew point in this figure

Once the aromaticity parameters are calculated for all pressure points, the aromaticity parameters are plotted with respect to pressure. Then, curve fitting is performed in the single-phase and two-phase regions separately. The intersection of the two fitting curves is determined as the saturation pressure of the mixture. Note that the method is not applicable to extremely light reservoir fluids with no C_{7+} fraction; however, CME is rarely performed for such simpler reservoir fluids.

4 | CASE STUDIES

In this section, the new method is verified first by using 15 black oils, for which the conventional PV-isotherm method can provide reliable saturation pressures. Then, it is tested for more challenging datasets

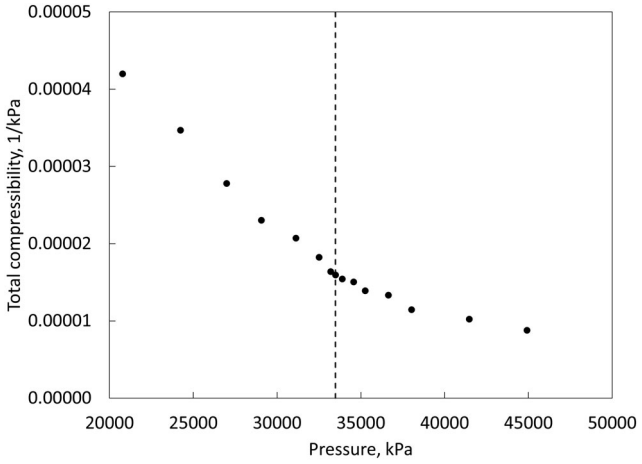

FIGURE 10 Total compressibility of fluid #8 in Table 3 (near-critical fluid) at 403.71 K23. The saturation pressure is indicated by the dashed line. Total compressibility does not show a clear change in slope at the dew point in this figure

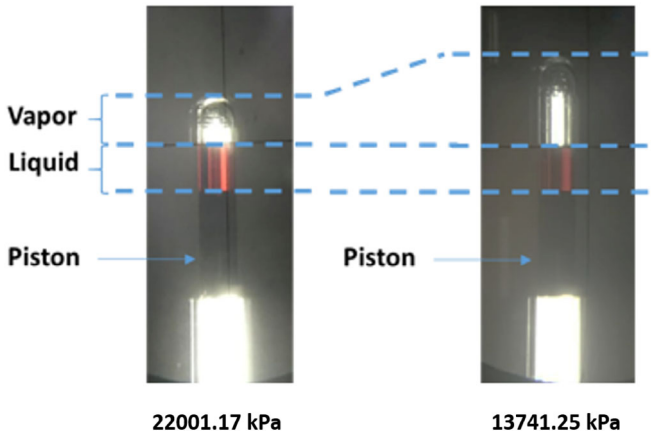

FIGURE 11 Snapshots of in-house constant-mass expansion for the mixture of 9.5 mol% CO2 and 90.5 mol% live oil from a shale play in Texas at 347.05 K. The expansion of the overall fluid comes mainly from the vapor phase [Color figure can be viewed at wileyonlinelibrary.com]

of 44 fluids, including volatile oils and gas condensates, and compared with the compressibility-based methods.

4.1 | Verification of the new method using black oil data

Table 1 lists the 15 black oils used for the verification of the new method. They include the data from swelling tests (Fluids #6–9 in Table 1) in addition to original reservoir fluids. The PV data from CME exhibit a clear change in slope at a saturation pressure for black oils; therefore, the saturation pressure determined by the authors using the PV-isotherm method is considered as a true saturation pressure in this subsection.

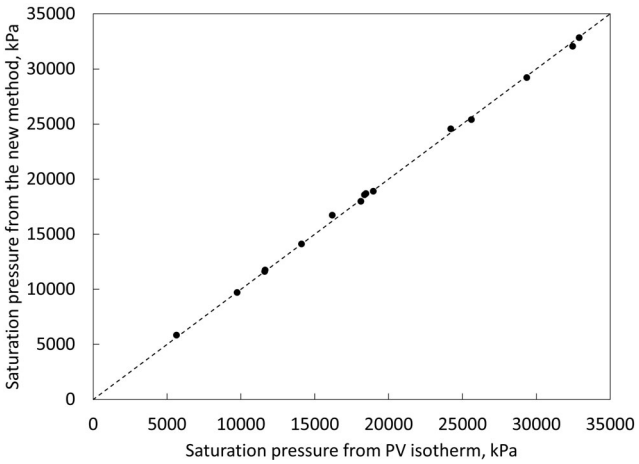

FIGURE 12 Comparison between the saturation pressures from PV isotherm (P_{sat_PV}) and those from the new method (P_{sat_new}) for the 15 black oils. Saturation pressures from the two methods are in good agreement with R^2 of 0.9991. The MAE between P_{sat_PV} and P_{sat_new} is 183 kPa, and the standard deviation of absolute error between P_{sat_PV} and P_{sat_new} is 154 kPa

Figure 12 compares the saturation pressures by the PV-isotherm method (P_{sat_PV}) with those by the new method (P_{sat_new}) for the 15 black oils. The two methods are in good agreement with a coefficient of determination (R^2) of 0.9991. The mean absolute error (MAE) and the standard deviation of absolute error between P_{sat_PV} and P_{sat_new} are 183 and 154 kPa, respectively. The absolute errors between P_{sat_PV} and P_{sat_new} are comparable to the uncertainty in the laboratory measurement, which is usually 100–200 kPa for bubble point pressure.[22] These results verify the new method for the determination of saturation pressure for black oils, and will be tested for more cases below.

4.2 | Testing of the new method and comparison with the conventional methods

Tables 2 and 3 show the 44 reservoir fluids (24 volatile oils and 20 gas condensates) used for testing the new method. They include data from swelling tests (Fluids 8–11 and 20–24 in Table 2 and Fluids 19 and 20 in Table 3) in addition to original reservoir fluids.

The method used for saturation pressures in the literature is the PV-isotherm method for Fluids 8–11 in Table 2 and the direct-observation method for Fluid 1 in Table 3. For the rest of the fluids in Tables 2 and 3, the method used to determine saturation pressures is not mentioned in the literature.

The saturation pressures determined by the new method (P_{sat_new}) are compared with the values reported in the literature ($P_{sat\_reported}$) in Figures 13 and 14 for volatile oils and gas condensates, respectively. Overall, the results from the new method are consistent with the data reported in the literature. The results for volatile oils in Figure 13 give the R^2 value of 0.9990. The MAE and the standard deviation of absolute error between P_{sat_new} and $P_{sat\_reported}$ for

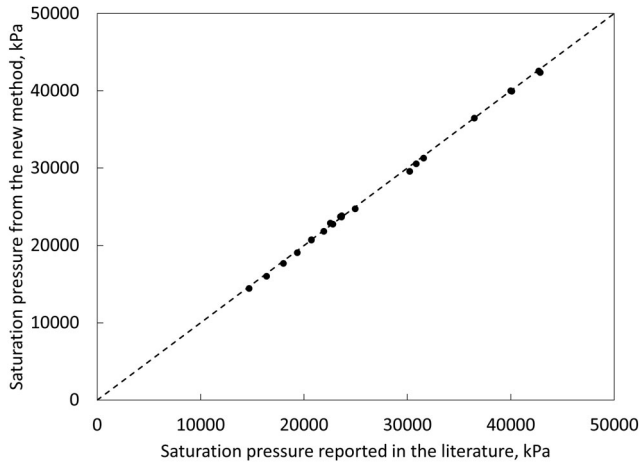

FIGURE 13 Comparison between the saturation pressures reported in the literature ($P_{sat\_reported}$) and those based on the new method (P_{sat_new}) for the 20 volatile oils (Fluids 20–23 in Table 2 are not included). There is a clear correlation with R^2 of 0.9990. The MAE and the standard deviation of absolute error between $P_{sat\_reported}$ and P_{sat_new} are 219 kPa and 168 kPa, respectively. Fluids 20–23 in Table 2 are not included in this figure because only the new method was used for in-house swelling tests

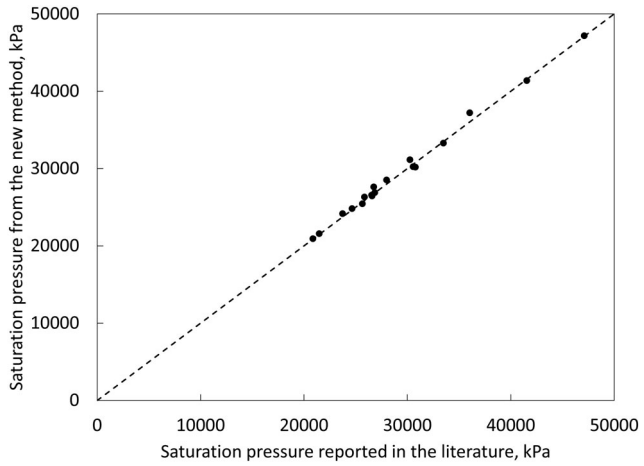

FIGURE 14 Comparison between the saturation pressures reported in the literature ($P_{sat\_reported}$) and those based on the new method (P_{sat_new}) for the 18 gas condensates. A clear correlation is observed with R2 of 0.9944. The MAE and the standard deviation of absolute error between $P_{sat\_reported}$ and P_{sat_new} are 360 and 342 kPa, respectively. Fluids 19 and 20 in Table 3 are not included in this figure because only the new method was used for in-house swelling tests

volatile oils are 219 and 168 kPa, respectively. The results for gas condensates in Figure 14 give the R^2 value of 0.9944. The MAE and the standard deviation of absolute error between P_{sat_new} and $P_{sat\_reported}$ for gas condensates are 360 and 342 kPa, respectively. The absolute errors between P_{sat_new} and $P_{sat\_reported}$ for both volatile oils and gas condensates are comparable to the uncertainty in the laboratory measurement (100–200 kPa for bubble point pressure and 100–1,000 kPa for dew point pressure).[22]

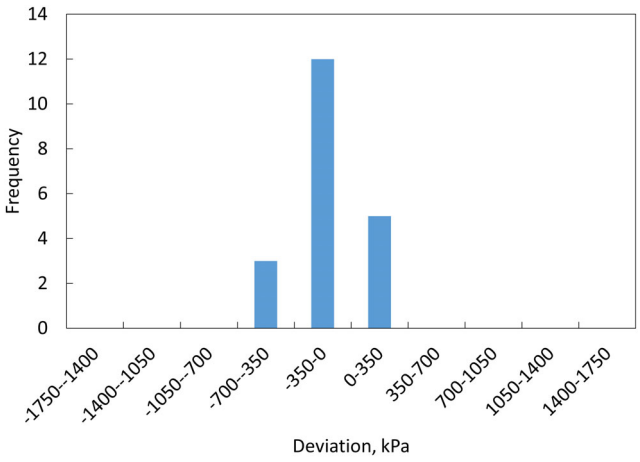

FIGURE 15 The histogram of deviations between P_{sat_new} and $P_{sat\_reported}$ for volatile oils. The distribution has a mean of −149 kPa, and a skewness of −0.0217. The distribution is nearly symmetric [Color figure can be viewed at wileyonlinelibrary.com]

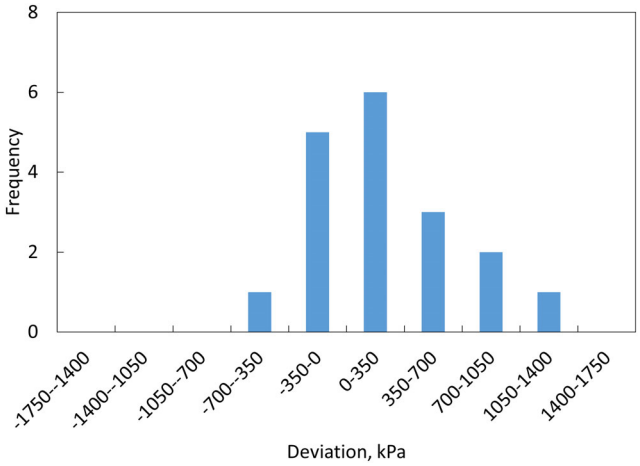

FIGURE 16 The histogram of deviations between P_{sat_new} and $P_{sat\_reported}$ for gas condensates. The distribution has a mean of −191 kPa, and a skewness of 0.6328. The distribution is asymmetric with the longer tail on the right side [Color figure can be viewed at wileyonlinelibrary.com]

Figures 15 and 16 present the histograms of deviations between P_{sat_new} and $P_{sat\_reported}$ (i.e., P_{sat_new}–$P_{sat\_reported}$) for volatile oils and gas condensates, respectively. The mean and skewness of the distribution in Figure 16 are 191 kPa and 0.6328, respectively. This positive skewness means asymmetric distribution with the tail on the right side. It is contributed by the positive deviations for 12 gas condensates out of the 18 samples reported in the literature; that is, the saturation pressures determined by the new method are greater than the reported values in the literature. This is most likely because the data reported in the literature are based on direct observation of the appearing phase. For gas condensate, the appearing liquid phase is likely to wet the interior of the PVT cell before forming a visible condensed phase, leading to an underestimated saturation pressure. In fact, such

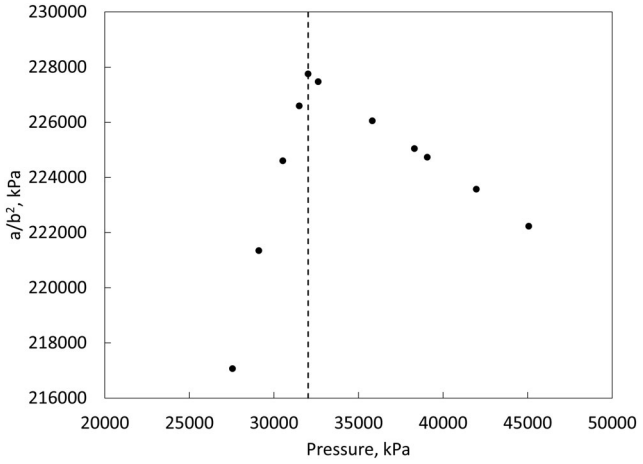

FIGURE 17 Aromaticity parameters calculated for fluid #9 in Table 1 (black oil) at 388.15 K[25]. The saturation pressure, which is indicated by the dashed line, is clearly determined with the slope-ratio value of −4.42

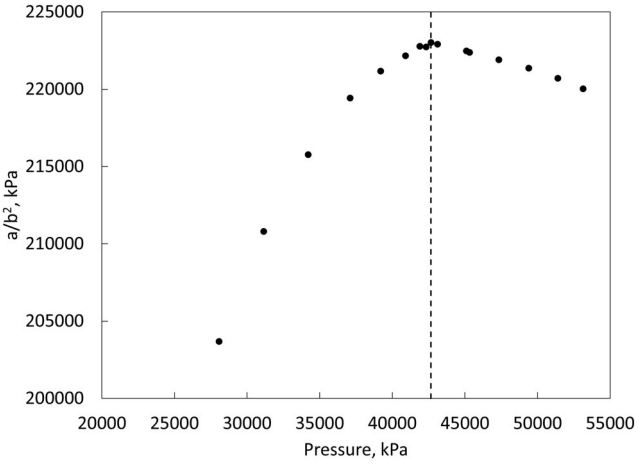

FIGURE 18 Aromaticity parameters calculated for fluid #11 in Table 2 (volatile oil) at 388.15 K[25]. The saturation pressure, which is indicated by the dashed line, is clearly determined with the slope-ratio value of −1.94

a bias was not observed for volatile oils (Figure 15). The distribution in Figure 15 has a mean of −149 kPa, and a skewness of −0.0217. This small skewness indicates that the distribution is almost symmetric, unlike in the condensate cases.

The application of the new method to 59 different fluids indicated that a linear relationship should be used in the single-phase region and a power series in the two-phase region for curve fitting. Therefore, the new method requires at least two points for the single-phase region and three points for the two-phase region. This makes the new method requires a small number of pressure steps (as small as five) during the CME test; hence, CME experiments can be done more efficiently by the new method.

The new method is compared with compressibility-based methods as summarized in Tables 1–3. The values of slope ratios for the new method are generally negative, no matter what the fluid type is. This makes it much easier to determine a saturation pressure with the new method than with the compressibility-based methods. No cases show a slope ratio between 0 and 2 with the new method, indicating that they are not difficult CME datasets for the new method. This is true also for Fluids #20–23 in Table 2 and Fluids #19 and #20 in Table 3, indicating that the new method has been successfully applied to the swelling test data.

Figures 17–20 present the aromaticity parameters for Fluid #9 in Table 1 (black oil), Fluid #11 in Table 2 (volatile oil), Fluid #18 in Table 3 (gas condensate), and Fluid #8 in Table 3 (near-critical fluid). They can be compared with Figures 1–4 (P-V isotherm) and Figures 5–8 (Y_{EXT}) to graphically demonstrate the advantage of the new method over the compressibility-based methods. Among these four fluids, Fluid #11 in Table 2, Fluid #18 in Table 3, and Fluid #8 in Table 3 were demonstrated as difficult cases with the compressibility-based methods. However, Figures 18–20 show that saturation pressures can be clearly determined by the new method with their slope-ratio values being all negative

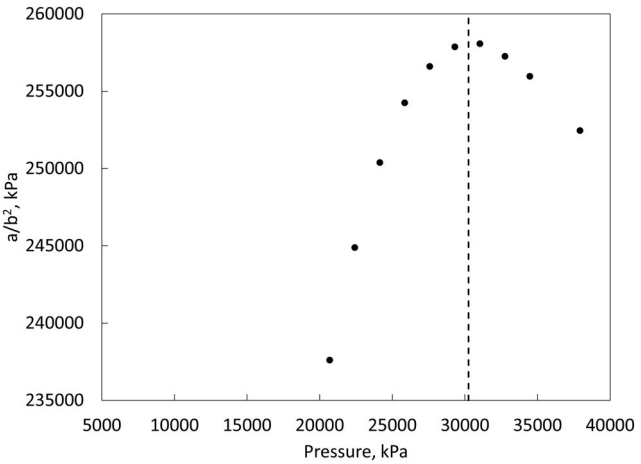

FIGURE 19 Aromaticity parameters calculated for fluid #18 in Table 3 (gas condensate) at 360.93 K[32]. The saturation pressure, which is indicated by the dashed line, is clearly determined with the slope-ratio value of −0.69

Among the 59 datasets, three datasets show positive slope ratios with the new method. The positive slope ratios are caused by a small positive slope of the aromaticity parameter in the single-phase region. However, the slope ratios for these cases are greater than 2, causing no difficulty in identifying a saturation point.

These results demonstrate that the new method is applicable with CME data for all types of reservoir fluids including swelling-test data. The new method is particularly effective in improving the problem with near-critical fluids, for which the compressibility-based methods are often unreliable. The reliability of the new method without depending on visual observation of an appearing phase can be useful particularly when visual observation is impossible with asphaltene precipitation and with extremely high pressure–temperature conditions.

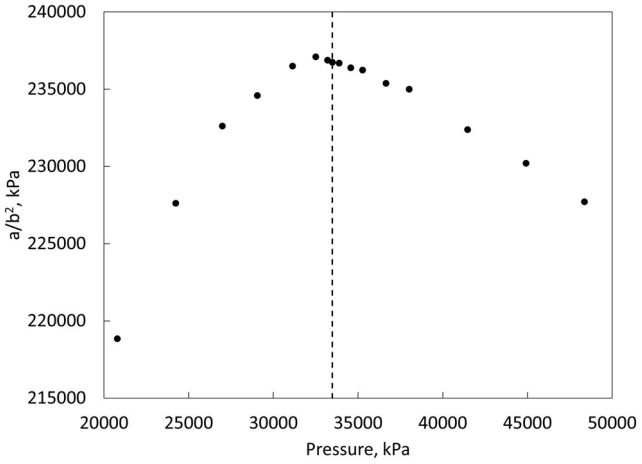

FIGURE 20 Aromaticity parameters calculated for fluid #8 in Table 3 (near-critical fluid) at 403.71 K[23]. The saturation pressure, which is indicated by the dashed line, is clearly determined with the slope-ratio value of −0.85

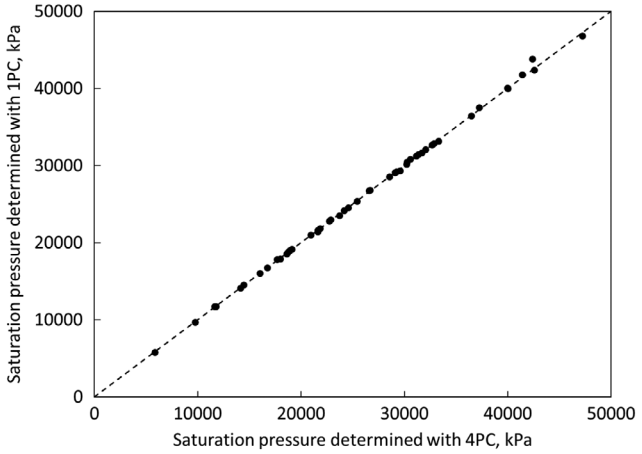

FIGURE 21 Comparison of the saturation pressures determine with one pseudo-component and four pseudo-components. This figure shows the consistency between the two cases, with R^2 of 0.9993. The MAE and the standard deviation of absolute error between P_{sat_1PC} and P_{sat_4PC} are 121 and 215 kPa, respectively. MAE, mean absolute error

4.3 | Number of pseudo-components used in the new method

The new method was successfully implemented by using four pseudo-components for the case studies in this article. The algorithm was also tested with one pseudo-component to study the impact on the saturation pressure determination. Figure 21 compares the resulting saturation pressures with one pseudo-component (P_{sat_1PC}) and four pseudo-components (P_{sat_4PC}). The data in Figure 21 gives the R^2 value of 0.9993. The MAE and the standard deviation of absolute error between P_{sat_1PC} and P_{sat_4PC} are 121 and 215 kPa, respectively. It shows the consistency between the two cases, but the use of one pseudo-component caused convergence issues at certain pressure steps, which may result in an insufficient amount of data for curve fitting. Among the 59 datasets tested, 11 datasets encountered convergence issues with one pseudo-component. Therefore, it is recommended that the new method is used with four pseudo-components as implemented in this research.

5 | CONCLUSIONS

A new method was developed for reliable determination of saturation pressure from CME data even when the total compressibility of the fluid does not show a detectable change near the saturation pressure. The method relies on the conversion of the expansion behavior of the overall fluid into compositional behavior information through the attraction and covolume parameters of the Peng–Robinson EOS. Using CME data for 59 different fluids, the hypothesis was successfully tested that when the fluid expansion is represented by the EOS as a single-phase mixture, the attraction and covolume parameters can capture the contribution of the more volatile phase to the fluid expansion. Specific conclusions are as follows:

- The case studies using 59 different fluids (20 gas condensates, 24 volatile oils, and 15 black oils) showed that the new method was superior to the previous methods for reliable determination of saturation pressure from CME data.
- The new method was the only method that could identify the saturation pressures for five volatile oils, 11 gas condensates, and one near-critical fluid among the datasets tested. The demonstrated reliability of the new method without depending on visual observation of an appearing phase can be useful particularly when visual observation is not possible with asphaltene precipitation and with extremely high pressure–temperature conditions.
- For 12 gas condensates, the dew point pressure determined by the new method was higher than the value reported in their original papers. This is most likely because the dew points reported in the literature are based on direct observation of the appearing liquid phase. The appearing liquid phase is likely to wet the interior of the PVT cell before forming a visible phase; hence, the direct observation tends to underestimate the dew point pressure. This bias was not observed for oils.
- The new method requires fewer pressure points for reliable determination of saturation pressure from CME. In principle, it is sufficient to obtain two data points for the single-phase region and three data points for the two-phase region when the new method is used to process CME data.
- It is recommended that the new method is used with four pseudo-components as in this article.

AUTHOR CONTRIBUTIONS

Mingyuan Wang: Conceptualization; data curation; formal analysis; investigation; methodology; software; validation; visualization; writing-original draft. **Francisco Argüelles-Vivas:** Data curation; supervision; visualization; writing-review and editing. **Ryosuke Okuno:** Conceptualization; formal analysis; funding acquisition; investigation; methodology; project

administration; resources; software; supervision; validation; visualization; writing-original draft; writing-review and editing.

DATA AVAILABILITY STATEMENT

The data that support the findings of this study are available from the corresponding author upon reasonable request.

NOMENCLATURE

Roman symbols

a	attraction parameter
b	covolume parameter
C	compressibility
f	function
i	indices
k	index
m	mass
n	number of moles
N	number
P	pressure in kPa
R	the gas constant
R^2	coefficient of determination
S	saturation
T	temperature in K
V	volume
Y	Y-function
Z	compressibility factor

Greek symbols

ω	acentric factor
ρ	density
Δ	variation
δ	tolerance

Subscripts

A	appearing phase
c	critical condition
E	existing phase
EXT	extended
H	aromatic equivalent
i	component
p	n-alkane equivalent
sat_new	saturation pressure based on the new method
sat_PV	saturation pressure from the PV isotherm
sat_reported	saturation pressure reported in the literature
sat_1PC	saturation pressure determined with 1 pseudo-component
sat_4PC	saturation pressure determined with 4 pseudo-components
t	total

Notation

BIP	binary interaction parameter
CME	constant-mass expansion
CN	carbon number
EOR	enhanced oil recovery
EOS	equation of state
MAE	mean absolute error
MW	molecular weight
PNA	paraffin-naphthenes-aromatics
PnA	perturbation from n-alkane
PV	pressure-volume
TOL	tolerance

ORCID

Ryosuke Okuno https://orcid.org/0000-0003-3675-1132

REFERENCES

1. Hosein R, Mayrhoo R, McCain WD Jr. Determination and validation of saturation pressure of hydrocarbon systems using extended Y-function. *J Petrol Sci Eng*. 2014;124:105-113. https://doi.org/10.1016/j.petrol.2014.10.022.
2. Odi U, El Hajj H, Gupta A. Experimental investigation of wet gas dew point pressure change with carbon dioxide concentration. Paper presented at: 2012 Abu Dhabi International Petroleum Conference and Exhibition, 11–14 Nov, Abu Dhabi, UAE SPE-161478-MS. https://doi.org/10.2118/161478-MS
3. Avaullee L, Trassy L, Neau E, Jaubert JN. Thermodynamic modeling for petroleum fluids I. equation of state and group contribution for the estimation of thermodynamic parameters of heavy hydrocarbons. *Fluid Phase Equilib*. 1997;139(1–2):155-170. https://doi.org/10.1016/S0378-3812(97)00168-4.
4. Peng DY, Robinson DB. A new two-constant equation of state. *Ind Eng Chem Fundam*. 1976;15(1):59-64. https://doi.org/10.1021/i160057a011.
5. Robinson DB, Peng DY. The characterization of the Heptanes and heavier fractions for the GPA Peng-Robinson programs. Gas processors association, Research report RR-28. 1978.
6. Soave G. Equilibrium constants from a modified Redlich-Kwong equation of state. *Chem Eng Sci*. 1972;27(6):1197-1203. https://doi.org/10.1016/0009-2509(72)80096-4.
7. Whitson CH, Brulé MR, Society of Petroleum Engineers. *Phase Behavior*. Richardson, TX: Henry L. Doherty Memorial Fund of AIME; 2000.
8. Pedersen KS, Christensen PL, Shaikh JA. *Phase Behavior of Petroleum Reservoir Fluids*. Boca Raton, FL: CRC Press, Taylor & Francis Group; 2015.
9. Kumar A, Okuno RA. New algorithm for multiphase-fluid characterization for solvent injection. *SPE J*. 2016;21(05):1-688.SPE-175123-PA. https://doi.org/10.2118/175123-PA.
10. Kumar A, Okuno R. Direct perturbation of the Peng–Robinson attraction and covolume parameters for reservoir fluid characterization. *Chem Eng Sci*. 2015;127:293-309. https://doi.org/10.1016/j.ces.2015.01.032.
11. Qian JW, Jaubert JN, Privat R. Phase equilibria in hydrogen-containing binary systems modeled with the Peng-Robinson equation of state and temperature-dependent binary interation parameters calculated through a group-contribution method. *J Supercrit Fluids*. 2013;75:58-71. https://doi.org/10.1016/j.supflu.2012.12.014.
12. Kumar A, Okuno R. Critical parameters optimized for accurate phase behavior modeling for heavy n-alkanes up to C100 using the Peng-Robinson equation of state. *Fluid Phase Equilib*. 2012;335:46-59. https://doi.org/10.1016/j.fluid.2012.07.029.
13. Alboudwarej H, Sheffield JM, Srivastava M, Wu SS, Zuo L, Inouye A, Zhou D, Oghena A. High pressure gas EOR PVT experimental

programs: challenges in measurements and data interpretations. Paper presented at: 2018 SPE Improved Oil Recovery Conference, 14–18 April, Tulsa, Oklahoma, USA. SPE-190257-MS. https://doi.org/10.2118/190257-MS
14. McCain WD Jr. The properties of petroleum fluids. *PennWell Corp*. Tulsa: Oklahoma: PennWell Corp; 2017.
15. Shaikh JA, Sah P. Experimental PVT data needed to develop EoS Model for EOR projects. Paper presented at: 2011 SPE Enhanced Oil Recovery Conference 19–21 July. Kuala Lumpur, Malaysia. SPE-144023-MS. https://doi.org/10.2118/144023-MS
16. Eyton DGP. Practical limitations in obtaining PVT data for gas condensate systems. Paper presented at: 1987 Middle East Oil Show Mar 7–10. Banama, Bahrain. SPE-15765-MS. https://doi.org/10.2118/15765-MS
17. Potsch KT, Braeuer L. A Novel graphical method for determining dewpoint pressures of gas condensates. Paper presented at: 1996 European Petroleum Conference Oct 22–24. Milan, Italy. SPE-36919-MS. https://doi.org/10.2118/36919-MS
18. Potsch K, Toplack P, Gumpenberger T. A review and extension of existing consistency tests for PVT data from a laboratory. *SPE Res Eval Eng*. 2017;20(02):269-284, SPE-183640-PA. https://doi.org/10.2118/183640-PA.
19. Kumar A, Okuno R. Characterization of reservoir fluids using an EOS based on perturbation from n-alkanes. *Fluid Phase Equilib*. 2013;358:250-271. https://doi.org/10.1016/j.fluid.2013.08.035.
20. Quiñones-Cisneros SE, Zéberg-Mikkelsen CK, Baylaucq A, Boned C. Viscosity modeling and prediction of reservoir fluids: from natural gas to heavy oils. *Int J Thermophys*. 2004;25(5):1353-1366. https://doi.org/10.1007/s10765-004-5743-z.
21. Jaubert JN, Privat R, Le Guennec Y, Coniglio L. Note on the properties altered by application of a péneloux-type volume translation to an equation of state. *Fluid Phase Equilib*. 2016;419:88-95. https://doi.org/10.1016/j.fluid.2016.03.012.
22. Meisingset KK. Uncertainties in reservoir fluid description for reservoir modeling. *SPE Res Eval Eng*. 1999;2(5):431-435.SPE-57886-PA. https://doi.org/10.2118/57886-PA.
23. Coats KH, Smart GT. Application of a regression-based EOS PVT program to laboratory data. *SPE Res Eng*. 1986;1(03):277-299.SPE-11197-PA. https://doi.org/10.2118/11197-PA.
24. Danesh A. *PVT and Phase Behaviour of Petroleum Reservoir Fluids*. Amsterdam, The Netherlands: Elsevier; 1998.
25. Jaubert JN, Avaullee L, Souvay JF. A crude oil data bank containing more than 5000 PVT and gas injection data. *J Petrol Sci Eng*. 2002;34(1–4):65-107. https://doi.org/10.1016/S0920-4105(02)00153-5.
26. Eilerts CK, Smith RV. Specific volumes and phase-boundary properties of separator-gas and liquid-hydrocarbon mixtures. Vol. 3642. US Department of the Interior, Bureau of Mines. 1942.
27. Negahban S, Pedersen KS, Sah P, Basioni MA, Azeem J. An EoS model for a Middle East reservoir fluid with an extensive EOR PVT data material. Paper presented at: 2010 Abu Dhabi International Petroleum Exhibition and Conference Nov 1–4. Abu Dhabi. SPE-136530-MS. https://doi.org/10.2118/136530-MS
28. Al-Meshari AA. New strategic method to tune equation-of-state to match experimental data for compositional simulation. Doctoral Dissertation, Texas A&M University. 2005.
29. Akpabio JU, Udofia EE, Ogbu M. PVT fluid characterization and consistency check for retrograde condensate reservoir modeling. Paper presented at: 2014 SPE Nigeria Annual International Conference and Exhibition Aug 5–7. Lagos, Nigeria. SPE-172359-MS. https://doi.org/10.2118/172359-MS
30. Coats KH. Simulation of gas condensate reservoir performance. *J Pet Technol*. 1985;37(10):1870-1886, SPE-10512-PA. https://doi.org/10.2118/10512-PA.
31. Kenyon DE, Behie GA. Third SPE comparative solution project: gas cycling of retrograde condensate reservoirs. *J Pet Technol*. 1987;39(08):981-997, SPE-12278-PA. https://doi.org/10.2118/12278-PA.
32. Sage BH, Olds RH. Volumetric behavior of oil and gas from several San Joaquin Valley fields. *Trans AIME*. 1947;170(01):156-173, SPE-947167-G. https://doi.org/10.2118/947156-G.
33. Williams JM. Why Y? Paper presented at: The 2011 SPE Annual Technical Conference and Exhibition Oct 30–2 Nov. Denver, Colorado, USA. SPE-146394-MS. https://doi.org/10.2118/146394-MS

How to cite this article: Wang M, Argüelles-Vivas FJ, Okuno R. Robust and efficient determination of saturation pressure from constant mass expansion data. *AIChE J*. 2021; e17166. https://doi.org/10.1002/aic.17166

APPENDIX A: Quality Control of CME Data

Y-function was used to confirm the quality of CME data in this research. It is defined as

$$Y = \frac{P_{sat} - P}{P\left(\frac{V}{V_{sat}} - 1\right)} \quad \text{(A-1)}$$

where P_{sat} is the saturation pressure, and V_{sat} is the fluid volume at P_{sat}.

Y-function is supposed to be a straight line or a line with only a small curvature in the two-phase region[33]. This research does not use any datasets that show obvious deviation from a straight line. Figures A-1 and A-2 illustrate low-quality and high-quality datasets, respectively, taken from Pedersen[8] and Fluid # 8 in Table 3. Figure A-1 shows deviation from a straight line, and Figure A-2 shows a line with only a small curvature, indicating high-quality data. Typical reasons for low-quality data include an insufficient period allowed for equilibration and insufficient mixing.

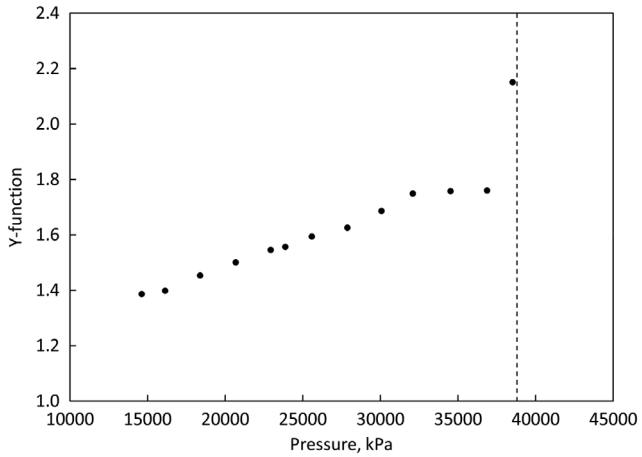

FIGURE A-1 Y-function at different pressures for CME data from Pedersen at 428.15 K[8]. Saturation pressure reported in the literature is indicated as dashed line. Y-function shows deviation from a straight line, indicating a low-quality CME dataset

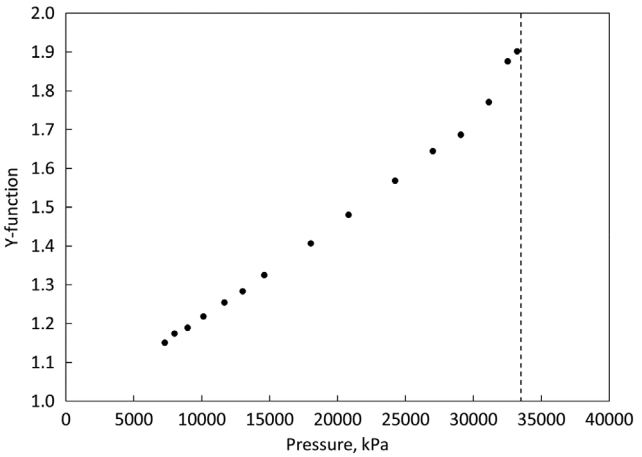

FIGURE A-2 Y-function at different pressures for CME data from fluid #8 in Table 3 at 403.71 K[23]. Saturation pressure reported in the literature is indicated as dashed line. Y-function shows a line with only a small curvature, indicating a high-quality CME dataset